MITSUBISHI ELECTRIC RESEARCH LABORATORIES
https://www.merl.com

Model Predictive Control Approach for Autonomous Sun-Synchronous Sub-Recurrent Orbit Control

Hayashi, Naohiro; Weiss, Avishai; Di Cairano, Stefano

TR2021-005 January 23, 2021

Abstract

In recent years, control of satellites without resorting to ground stations, i.e., autonomous satellite control, has attracted significant interest due to the potential of providing high precision, flexibility, and reduced operating costs. In this paper we consider the autonomous satellite control in a Sun-synchronous Sub-recurrent orbit (SSO), in Very Low Earth Orbit (VLEO). We propose a linear time-varying Model Predictive Control (MPC) for SSO formulated based on Relative Orbital Elements (ROE). The MPC capabilities of handling multi-input multi-output systems subject to constraints, its predictive nature, and the usage of ROE in the cost function enables to control SSO keeping and transferring based on the ground trace, while also accounting for coasting phases where propulsion should not be engaged. The proposed method also has limited computational burden, since linear MPC requires solving a convex quadratic program for which efficient and compact solvers exists. We assess the performance of the proposed method by simulations in closed-loop with both, a nonlinear model of the satellite orbital dynamics and the GMAT simulation toolkit.

AIAA SciTech

Mitsubishi Electric Research Laboratories, Inc.
201 Broadway, Cambridge, Massachusetts 02139

Model Predictive Control Approach for Autonomous Sun-Synchronous Sub-Recurrent Orbit Control

Naohiro Hayashi*, Avishai Weiss† and Stefano Di Cairano‡

In recent years, control of satellites without resorting to ground stations, i.e., autonomous satellite control, has attracted significant interest due to the potential of providing high precision, flexibility, and reduced operating costs. In this paper we consider the autonomous satellite control in a Sun-synchronous Sub-recurrent orbit (SSO), in Very Low Earth Orbit (VLEO). We propose a linear time-varying Model Predictive Control (MPC) for SSO formulated based on Relative Orbital Elements (ROE). The MPC capabilities of handling multi-input multi-output systems subject to constraints, its predictive nature, and the usage of ROE in the cost function enables to control SSO keeping and transferring based on the ground trace, while also accounting for coasting phases where propulsion should not be engaged. The proposed method also has limited computational burden, since linear MPC requires solving a convex quadratic program for which efficient and compact solvers exists. We assess the performance of the proposed method by simulations in closed-loop with both, a nonlinear model of the satellite orbital dynamics and the GMAT simulation toolkit.

I. Introduction

SUN-SYNCHRONOUS Sub-recurrent Orbit (SSO), in which a satellite passes over the same ground trace at the same Local Solar Time (LST), is one of the most commonly used orbits. SSO is useful for communication and observation, and the keeping of ground trace and LST are the most important quality factors in SSO satellites. In recent missions, more accurate SSO control has been required. For instance, in the case of the RADARSAT Constellation Mission (RCM), which was launched by the Canadian Space Agency (CSA) in 2019, the three satellites are required to fly in an orbital tube of radius 100 m while keeping a specific LST [1, 2].

In addition, in recent years the utilization of Very Low Earth Orbit (VLEO) has also been investigated. In 2017, the Japan Aerospace Exploration Agency (JAXA) and Mitsubishi Electric Corporation launched a 400-kg-class satellite called Super Low Altitude Test Satellite (SLATS). SLATS demonstrated orbit control at an altitude of 167.4 km using an ion thruster and a reaction control system [3–5]. In general, VLEO satellites have several advantages such as increased gain and reduced power consumption in communications, and increased resolution with smaller sensors in observations. Also, VLEO satellites may be launched by smaller and less expensive vehicles. For these reasons, VLEO holds significant potential by achieving high performance and cost reduction of earth orbiting satellites.

However, the lower the altitude satellites fly at, the more severe the air drag effects are. According to the U.S. Standard Atmosphere 1976, the air density at an altitude of 200 km is about a thousand times higher than that of a typical low Earth orbit at an altitude of 600 km (Fig. 1) [6]. Due to such high air density, there are two challenges for orbit control in VLEO. The first one is high propellant consumption, as propellant is consumed proportionally to air density. To remedy that, a possibility is to use ion thrusters that have high specific impulse. The second challenge is the requirement for frequent and accurate control. In a conventional system, orbit control is conducted by a ground station. Since ground-based control involves many steps, such as propagating the orbit from GPS signals, scheduling thruster ignition while avoiding conflict with mission execution, and errors are accumulated from planning to execution, it is challenging to control VLEO orbits with the required frequency and accuracy. However, this challenge is significantly mitigated if the VLEO operation is controlled from on-board the satellite, i.e., autonomous satellite control is implemented.

In order to realize autonomous SSO satellite control in VLEO, we propose a Linear Time-Varying (LTV) Model Predictive Control (MPC) with a prediction model based on Relative Orbital Elements (ROE) that uses the linear mapping from Cartesian coordinates to ROE proposed in [7]. Since the ground trace of the SSO is geometrically represented by the orbital elements, the LTV-MPC with cost function expressed in terms of ROE enables control of SSO based on the ground trace.

*Satellite Engineer, Mitsubishi Electric Corporation, Kamakura Works, Kamimachiya, Kamakura, Kanagawa 247-8520, Japan.
†Principal Research Scientist, Mitsubishi Electric Research Laboratories, Cambridge, MA 02139, USA.
‡Distinguished Research Scientist, Mitsubishi Electric Research Laboratories, Cambridge, MA 02139, USA.

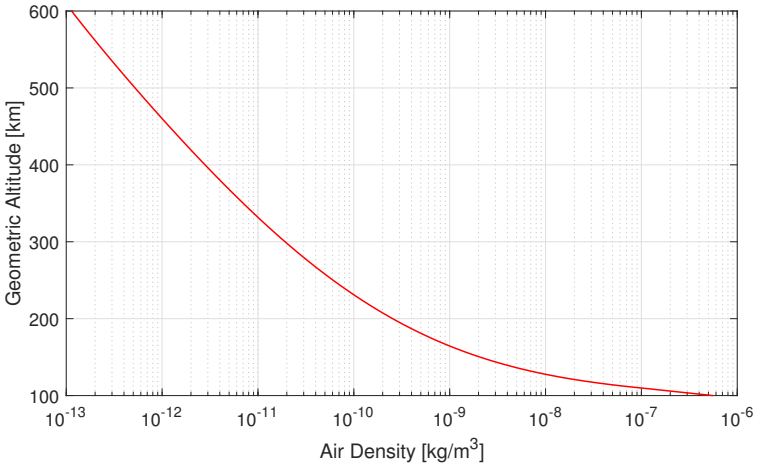

Fig. 1 Geometric altitude versus air density

LTV-MPC appears suitable for SSO control due to the following three features. First, MPC has the capability of handling constraints and can exploit prediction of disturbances along its prediction horizon. In MPC, the SSO orbital tube can be regarded as constraints, and also, thruster ignition can be scheduled based on predicted mission operations. Second, MPC computes a finite horizon optimal control solution for a multi-input multi-output system. In the orbit control system, the inputs are the three dimensional forces by thruters, and the outputs are the six orbital elements. Third, the LTV-MPC can be executed in embedded control platform with a limited computational burden [8]. In fact, for a linear (time-varying) prediction model and constraints, and a positive definite quadratic cost function, MPC requires only solving convex quadratic programs for which many algorithms with different degrees of performance and computational requirements exist.

MPC is considered a promising approach for autonomous guidance, navigation, and control of spacecraft. In a recent survey [9], several applications and methodologies of MPC for aerospace systems are reviewed and analyzed. In [10, 11], the authors discussed MPC-based rendezvous and docking under constraints including sensor line-of-sight cone, soft docking, attitude motion and obstacle avoidance. In [12, 13], the authors developed MPC for geostationary satellite station keeping coupled with attitude control and momentum management using electric thrusters, and in [14], LTV-MPC was used for a similar application on Earth-Moon L2 halo orbits. A large number of prior research on MPC applications to aerospace systems is reported in recent publications [8, 9].

In this paper we develop the linear MPC-based SSO keeping and transferring where the cost function is formulated based on the ROE. By approximating the nominal orbit as circular and Keplerian along the short prediction horizon of MPC, the satellite orbit is expressed by the Hill-Clohessy-Wiltshire (HCW) equations with respect to such nominal orbit. The HCW equations are linearized to obtain the satellite dynamics in Cartesian coordinates, and the linear-time varying mapping transforming the Cartesian coordinates into ROEs provides the performance outputs weighted in the cost function, so that the MPC optimal solution minimizes the ground trace error. Since SSO is obtained by exploiting the J_2 term of the Earth gravitational perturbation, MPC must reject the air drag effects, yet at the same time it must retain the effects of the J_2 Earth gravitational perturbation. We solve this problem by introducing an ephemeris which does not require re-propagation and re-uplink and by exploiting it for generating the target for MPC. The MPC is verified by numerical simulation, first based on the standard nonlinear model of the orbital dynamics using simple disturbance models, and then using the General Mission Analysis Tool (GMAT), which has been developed, verified and validated by National Aeronautics and Space Administration (NASA) Goddard Space Flight Center (GSFC) [15, 16]. In GMAT, the MPC is validated under a detailed atmospheric and geopotential model.

The rest of the paper is structured as follows. The simulation and MPC prediction models are introduced in Section II, the control design is introduced in Section III, the numerical simulations are reported in Section IV, and our conclusions are discussed in Section V.

II. SSO Satellite Models for Simulation and Control Design

A. Equations of Motion

The equations of motion for the Earth orbiting satellite with respect to the Earth-Centered Inertial (ECI) frame are given by

$$\ddot{\mathbf{r}} = -\mu \frac{\mathbf{r}}{|\mathbf{r}|^3} + \mathbf{f}, \tag{1}$$

where $\mathbf{r} \in \mathbb{R}^3$ is the position vector, μ is the geocentric gravitational constant, and $\mathbf{f} \in \mathbb{R}^3$ is the vector of external force per unit mass of the satellite, representing the thrusters and orbital perturbations acting on the satellite.

The exact linearization of (1) on SSO should include non-Keplerian perturbations and consider a non-zero eccentricity [17, 18]. In order to develop a prediction model for MPC, we make the approximations of considering a circular nominal orbit, and of neglecting the effects of the non-Keplerian perturbations. Since the prediction model based on such approximations is integrated only along the relatively short prediction horizon of MPC before being reset based on actual data, the effects of the non-Keplerian perturbations are small along such short horizon, and the SSO has small eccentricity, these approximations are appropriate for the prediction model of MPC. On the other hand, for computing the satellite target and for the numerical simulation of its orbit, we use (1) not to neglect the above effects.

Under the stated approximations the relative position vector of the satellite can be expressed with respect to the rotating frame (Hill's frame) in a circular nominal orbit (chief orbit) as

$$\mathbf{r}_\mathrm{d} = \mathbf{r} - \mathbf{r}_\mathrm{c}, \tag{2}$$

where $\mathbf{r}_\mathrm{c} \in \mathbb{R}^3$ is the position vector of the origin of Hill's frame, and the subscripts c and d indicate the origin (chief) in the circular orbit and satellite (deputy) respectively. For $|\mathbf{r}_\mathrm{d}| \ll |\mathbf{r}_\mathrm{c}|$, the relative motion of the satellite can be linearized to the HCW equations

$$\mathbf{x}'(\tau) = \mathbf{A}\mathbf{x}(\tau) + \mathbf{B}\mathbf{f}(\tau), \tag{3}$$

where the prime $'$ indicates differentiation with respect to the mean anomaly of the chief circular orbit $\tau = n_\mathrm{c} t$, $\mathbf{x} = [x \;\; y \;\; z \;\; x' \;\; y' \;\; z']^\mathrm{T}$ is the vector of relative positions and relative velocities of the satellite with respect to Hill's frame, and

$$\mathbf{A} = \begin{bmatrix} 0 & 0 & 0 & 1 & 0 & 0 \\ 0 & 0 & 0 & 0 & 1 & 0 \\ 0 & 0 & 0 & 0 & 0 & 1 \\ 3 & 0 & 0 & 0 & 2 & 0 \\ 0 & 0 & 0 & -2 & 0 & 0 \\ 0 & 0 & -1 & 0 & 0 & 0 \end{bmatrix}, \quad \mathbf{B} = \frac{1}{n_\mathrm{c}} \begin{bmatrix} \mathbf{0} \\ \mathbf{I} \end{bmatrix},$$

where $n_\mathrm{c} = \sqrt{\dfrac{\mu}{|\mathbf{r}_\mathrm{c}|^3}}$ is the mean motion of the chief circular orbit. By formulating the HCW equations as a differential equation of τ, the positions and velocities in Hill's frame can be transformed into ROE by a linear time-varying mapping [7, 19] as shown next.

B. Relative Orbital Elements

Relative orbital elements are one way of representing relative motion with respect to the Hill's frame and a linear (time-varying) mapping from the Cartesian coordinates of the HCW equations state to ROE exists [7, 20, 21]. ROE have been previously utilized for relative orbital motion control and formation flying [22, 23]. The ROE are defined as

$$\mathbf{z}(\tau) = a_\mathrm{c} \begin{bmatrix} \Delta a/a_\mathrm{c} \\ \Delta\lambda \\ \Delta e_x \\ \Delta e_y \\ \Delta i_x \\ \Delta i_y \end{bmatrix} = a_\mathrm{c} \begin{bmatrix} (a_\mathrm{d} - a_\mathrm{c})/a_\mathrm{c} \\ \phi_\mathrm{d} - \phi_\mathrm{c} + (\Omega_\mathrm{d} - \Omega_\mathrm{c}) \cos i_\mathrm{c} \\ e_{\mathrm{d}x} - e_{\mathrm{c}x} \\ e_{\mathrm{d}y} - e_{\mathrm{c}y} \\ i_\mathrm{d} - i_\mathrm{c} \\ (\Omega_\mathrm{d} - \Omega_\mathrm{c}) \sin i_\mathrm{c} \end{bmatrix}, \tag{4}$$

where Δa is the relative semi-major axis, $\Delta\lambda$ is the relative longitude, Δe_x and Δe_y are the components of the relative eccentricity vector, and Δi_x and Δi_y are the components of the relative inclination vector. Also, a is the semi-major axis, ϕ is the argument of latitude, Ω is the Right Ascension of Ascending Node (RAAN), i is the inclination, e is the eccentricity. The Hill's frame and ROE are shown in Fig. 2.

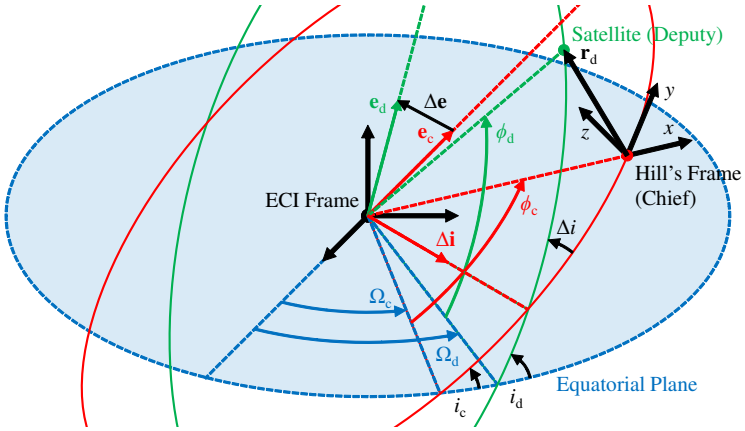

Fig. 2 Hill's frame and relative orbital elements

The transformation from the state in the HCW equations to the ROE is expressed as

$$\mathbf{z}(\tau) = \mathbf{E}(\tau)\mathbf{x}(\tau), \tag{5}$$

where

$$\mathbf{E}(\tau) = \begin{bmatrix} 4 & 0 & 0 & 0 & 2 & 0 \\ 0 & 1 & 0 & -2 & 0 & 0 \\ 3\cos\tau & 0 & 0 & \sin\tau & 2\cos\tau & 1 \\ 3\sin\tau & 0 & 0 & -\cos\tau & 2\sin\tau & 0 \\ 0 & 0 & \sin\tau & 0 & 0 & \cos\tau \\ 0 & 0 & -\cos\tau & 0 & 0 & \sin\tau \end{bmatrix}, \tag{6}$$

is the linear time-varying mapping transforming the HCW equations state into ROE.

C. Ground Trace Tracking Condition

In order to develop ground-trace-based control, we determine the conditions according to which the satellite tracks the ground trace of the target orbit. When formulating the conditions with respect to ROEs, these result to be linear conditions. From the definition (4), the relative argument of latitude and relative RAAN are expressed as

$$\begin{cases} \Delta\phi = \Delta\lambda - \Delta\Omega\cos i_c \\ \Delta\Omega = \dfrac{\Delta i_y}{\sin i_c}. \end{cases} \tag{7}$$

Geometrically, the ground trace tracking conditions are expressed as

$$\begin{cases} \Delta a = 0 \\ \Delta e_x = 0 \\ \Delta e_y = 0 \\ \Delta i_x = 0 \\ \dfrac{\Delta\phi}{n_c} + \dfrac{\Delta\Omega}{n_{\text{Erot}} - n_{\text{Erev}}} = 0, \end{cases} \tag{8}$$

where n_{Erot} is the angular velocity of Earth's rotation about its axis and n_{Erev} is the angular velocity of Earth's revolution about the Sun.

The fifth condition in (8) relates the angular movement of the deputy $\Delta\phi$ to that of Earth $\Delta\Omega$, ensuring that the ground trace below the target is moved to the nadir of the deputy by Earth's rotation, as shown in Fig. 3. From (7), the fifth condition is re-formulated as

$$n_{\mathrm{g}}\Delta\lambda + \Delta i_y = 0, \tag{9}$$

where $n_{\mathrm{g}} = \dfrac{(n_{\mathrm{Erot}} - n_{\mathrm{Erev}})\sin i_{\mathrm{c}}}{n_{\mathrm{c}} - (n_{\mathrm{Erot}} - n_{\mathrm{Erev}})\cos i_{\mathrm{c}}}$.

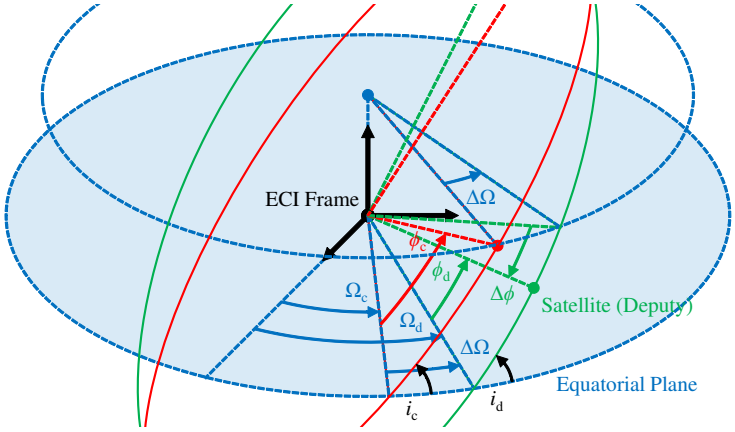

Fig. 3 Ground trace tracking condition

D. Perturbations

In the SSO, the dominant perturbations are air drag and Earth's anisotropic geopotential. The air drag applied to the satellite with respect to the Earth-Centered Rotational (ECR) frame is given by

$$\mathbf{f}_{\mathrm{air}} = -\frac{1}{2}\rho|\dot{\mathbf{r}}|^2 C_{\mathrm{drag}}\frac{A_{\mathrm{area}}}{m}\frac{\dot{\mathbf{r}}}{|\dot{\mathbf{r}}|}, \tag{10}$$

where ρ is the air density, C_{drag} is the drag coefficient, A_{area} is the cross-sectional area, and m is the mass of the satellite.

The J_2 term of the Earth gravitational perturbation causes a secular perturbation on the RAAN [18]. The secular perturbation of RAAN by J_2 is given by

$$\dot{\Omega} = -\frac{3J_2 n}{2(1-e^2)^2}\left(\frac{a_{\mathrm{E}}}{a}\right)^2\cos i, \tag{11}$$

where a_{E} is the Earth equatorial radius. Also, the resonance of J_2 and J_3 causes a secular perturbation on the eccentricity and argument of perigee [18]. These secular perturbations are given by

$$\begin{cases} \dot{e} = -\dfrac{3J_3 n}{2(1-e^2)^2}\left(\dfrac{a_{\mathrm{E}}}{a}\right)^3 \sin i\left(1 - \dfrac{5}{4}\sin^2 i\right)\cos\omega \\ \dot{\omega} = \dfrac{3J_3 n}{(1-e^2)^2}\left(\dfrac{a_{\mathrm{E}}}{a}\right)^2 \sin i\left(1 - \dfrac{5}{4}\sin^2 i\right)\left(1 + \dfrac{J_3}{2J_2(1-e^2)}\dfrac{a_{\mathrm{E}}}{a}\dfrac{\sin i\sin\omega}{e}\right). \end{cases} \tag{12}$$

Other perturbations such as the gravity of the Sun, the Moon and the other planets also influence the SSO, albeit their effects are smaller than the previously described perturbations. While detailed models for those can be obtained, in this paper they are regarded as unmodeled disturbances that the satellite controller compensates for by feedback.

E. Sun-synchronous Sub-recurrent and Frozen Condition

In a sun-synchronous orbit, the orbital plane rotates by 360 degree in each sidereal year. The sun-synchronous condition is expressed as

$$n_{\mathrm{Erev}} = \dot{\Omega}. \tag{13}$$

In a sub-recurrent orbit, the ratio of the satellite revolution to the Earth rotation is a rational number, which implies that the satellite repeats its ground trace. The sub-recurrent condition is expressed as

$$n = M(n_{\mathrm{Erot}} - \dot{\Omega}), \tag{14}$$

where $M \in \mathbb{Q}$ is the number of revolutions per day. The SSO is an orbit which has both features, i.e., it satisfies (13) and (14). To avoid consuming fuel for rotating the orbital plane, the SSO secular perturbation of RAAN obtained from (11) is used to satisfy (13) and (14) by appropriately determining a and i. In this way, the SSO is generated by J_2, i.e., the perturbation is actually exploited to achieve the desired orbit.

Although the secular perturbation of the eccentricity vector (12) is not dominant, over long periods it perturbs the SSO and causes propellant consumption. In order to avoid that, the SSO is designed to be a frozen orbit, where the eccentricity vector is fixed. Since $\dot{e}$ and $\dot{\omega}$ are given by (12), the frozen condition is expressed as

$$\begin{cases} e = -\dfrac{J_3 a_{\mathrm{E}}}{2J_2 a} \sin i \\ \omega = \dfrac{\pi}{2}. \end{cases} \tag{15}$$

When e and ω satisfy (15), the secular perturbation of the eccentricity vector does not perturb the SSO.

Summarizing, in this paper the target orbit is selected to satisfy the conditions (13), (14) and (15), and the chief circular orbit is selected to have the same semi-major axis (the same orbital period) as the target orbit.

III. Model Predictive Control Design

A. Prediction model for SSO Keeping

The general form of LTV prediction model for the MPC is the discrete time model given by

$$\begin{cases} \bar{\mathbf{x}}_{k+1} = \bar{\mathbf{A}}_k \bar{\mathbf{x}}_k + \bar{\mathbf{B}}_k \bar{\mathbf{u}}_k \\ \bar{\mathbf{y}}_k = \bar{\mathbf{C}}_k \bar{\mathbf{x}}_k + \bar{\mathbf{D}}_k \bar{\mathbf{u}}_k \\ \bar{\mathbf{z}}_k = \bar{\mathbf{E}}_k \bar{\mathbf{x}}_k, \end{cases} \tag{16}$$

where $\bar{\mathbf{x}}_k$, $\bar{\mathbf{y}}_k$, $\bar{\mathbf{z}}_k$ and $\bar{\mathbf{u}}_k$ are the state, constrained output, performance output, and input vector at the sampling instant $k \in \mathbb{N}$, respectively. For controlling the satellite motion described by (1), in this paper we build the prediction model (16) based on the HCW equations (3) that approximate (1), and we define the performance output vector by the ROE (4), (5). For (3), (4), (5), the vectors and matrices in (16) are

$$\bar{\mathbf{x}}_k = \mathbf{x}(\tau_k), \quad \bar{\mathbf{y}}_k = \mathbf{z}(\tau_k), \quad \bar{\mathbf{z}}_k = \mathbf{z}(\tau_k), \quad \bar{\mathbf{u}}_k = \mathbf{u}(\tau_k),$$

$$\bar{\mathbf{A}}_k = \mathbf{A}_{\mathrm{D}}, \quad \bar{\mathbf{B}}_k = \mathbf{B}_{\mathrm{D}},$$

$$\bar{\mathbf{C}}_k = \mathbf{E}(\tau_k), \quad \bar{\mathbf{D}}_k = \mathbf{0}, \quad \bar{\mathbf{E}}_k = \mathbf{E}(\tau_k),$$

where $\mathbf{u} \in \mathbb{R}^3$ is the thrust, $\mathbf{A}_{\mathrm{D}} \in \mathbb{R}^{6\times 6}$ and $\mathbf{B}_{\mathrm{D}} \in \mathbb{R}^{6\times 3}$ are the matrices obtained of the discrete-time representation of (3), and τ_k indicates mean anomaly of the chief at the k sampling period. However, this base prediction model is extended with additional ancillary states and dynamics. In order to achieve offset-free tracking of the orbit in the presence of disturbances, we introduce a disturbance prediction model, formulate the control input in incremental form, and add integral action on the performance output. The matrices and vectors of the resulting prediction model (16) are

$$\bar{\mathbf{x}}_k = [\mathbf{x}(\tau_k)^{\mathrm{T}} \ \mathbf{f}_{\mathrm{a}}^{\mathrm{T}} \ \mathbf{u}(\tau_{k-1})^{\mathrm{T}} \ \boldsymbol{\iota}(\tau_k)^{\mathrm{T}}]^{\mathrm{T}}, \quad \bar{\mathbf{y}}_k = [\mathbf{z}(\tau_k)^{\mathrm{T}} \ \mathbf{u}(\tau_k)^{\mathrm{T}}]^{\mathrm{T}},$$

$$\bar{\mathbf{z}}_k = [\mathbf{z}(\tau_k)^{\mathrm{T}} \ \boldsymbol{\iota}(\tau_k)^{\mathrm{T}}]^{\mathrm{T}}, \quad \Delta\bar{\mathbf{u}}_k = \mathbf{u}(\tau_k) - \mathbf{u}(\tau_{k-1}),$$

$$\bar{\mathbf{A}}_k = \begin{bmatrix} \mathbf{A}_{\mathrm{D}} & \mathbf{B}_{\mathrm{D}} & \mathbf{B}_{\mathrm{D}} & \mathbf{0} \\ \mathbf{0} & \mathbf{I} & \mathbf{0} & \mathbf{0} \\ \mathbf{0} & \mathbf{0} & \mathbf{I} & \mathbf{0} \\ \mathbf{E}(\tau_k) & \mathbf{0} & \mathbf{0} & \mathbf{I} \end{bmatrix}, \quad \bar{\mathbf{B}}_k = \begin{bmatrix} \mathbf{B}_{\mathrm{D}} \\ \mathbf{0} \\ \mathbf{I} \\ \mathbf{0} \end{bmatrix},$$

$$\bar{\mathbf{C}}_k = \begin{bmatrix} \mathbf{E}(\tau_k) & \mathbf{0} & \mathbf{0} & \mathbf{0} \\ \mathbf{0} & \mathbf{0} & \mathbf{I} & \mathbf{0} \end{bmatrix}, \quad \bar{\mathbf{D}}_k = \begin{bmatrix} \mathbf{0} \\ \mathbf{I} \end{bmatrix}, \quad \bar{\mathbf{E}}_k = \begin{bmatrix} \mathbf{E}(\tau_k) & \mathbf{0} & \mathbf{0} & \mathbf{0} \\ \mathbf{0} & \mathbf{0} & \mathbf{0} & \mathbf{I} \end{bmatrix},$$

where $\mathbf{f}_\mathrm{a} \in \mathbb{R}^3$ is the predicted disturbance which is assumed constant in the prediction horizon, $\Delta\bar{\mathbf{u}} \in \mathbb{R}^3$ is the thrust increment with respect to a previous step, and $\boldsymbol{\iota} \in \mathbb{R}^6$ is the integral of the performance output $\mathbf{z}$. Since $\mathbf{f}_\mathrm{a}$ cannot be directly measured, it must be estimate. While there are many ways to assume the disturbance, here we estimate $\mathbf{f}_\mathrm{a}$ from observed effects at the previous step,

$$\mathbf{f}_\mathrm{a} = \tilde{\mathbf{B}}_\mathrm{D}^{-1}(\tilde{\mathbf{x}}(\tau_k) - \tilde{\mathbf{A}}_\mathrm{D}\tilde{\mathbf{x}}(\tau_{k-1})) - \mathbf{u}(\tau_{k-1}), \tag{17}$$

where the tilde ˜ indicates lower half part of the matrix or vector, i.e., $\tilde{\mathbf{x}} = [x' \;\; y' \;\; z']^\mathrm{T}$.

For the controller to minimize the ground trace tracking error, we modify the performance output to represent the left hand side of (8), where the fifth condition is modified into (9). As a result we replace $\mathbf{E}$ by

$$\mathbf{E}_\mathrm{g}(\tau) = \begin{bmatrix} 1 & 0 & 0 & 0 & 0 & 0 \\ 0 & 1 & 0 & 0 & 0 & 0 \\ 0 & 0 & 1 & 0 & 0 & 0 \\ 0 & 0 & 0 & 1 & 0 & 0 \\ 0 & 0 & 0 & 0 & 1 & 0 \\ 0 & n_\mathrm{g} & 0 & 0 & 0 & 1 \end{bmatrix} \mathbf{E}(\tau), \tag{18}$$

According to $\mathbf{E}_\mathrm{g}$, the performance output $\mathbf{z}$ becomes

$$\mathbf{z}_\mathrm{g}(\tau) = a_\mathrm{c}[\Delta a/a_\mathrm{c} \;\; \Delta\lambda \;\; \Delta e_x \;\; \Delta e_y \;\; \Delta i_x \;\; n_\mathrm{g}\Delta\lambda + \Delta i_y]^\mathrm{T},$$

The initial state of the MPC controller is obtained from (1) based on the following transformations, that correct for the approximations in using the HCW equations (3) as prediction model instead of (1). First, since the SSO plane rotates 360 degrees in each sidereal year, whereas the Hill's frame orbital plane (chief orbital plane) is fixed in the ECI frame, the orbital plane in Hill's frame is rotated by the same angle as the SSO plane. Here, the inertial force by the rotation is ignored, considering that the error of such an approximation is relatively small and will be compensated by the feedback action of the controller. Second, while the air drag must be cancelled, the Earth gravitational perturbation must not be cancelled since it provides the secular perturbation needed by the SSO. Thus, an ephemeris, which contains the time series of target position and velocity is propagated under the Earth gravitational perturbation, and the difference between the state in (1) and ephemeris is used as in the initial state of the MPC prediction model. Thus, the state of the MPC prediction model $x(\tau)$ is

$$\mathbf{x}(\tau) = \begin{bmatrix} \mathbf{R}_I^H(t) & \mathbf{0} \\ \mathbf{0} & \dfrac{1}{n_\mathrm{c}}\mathbf{R}_I^H(t) \end{bmatrix} \begin{bmatrix} \mathbf{r}(t) - \mathbf{r}_\mathrm{e}(t) \\ (\dot{\mathbf{r}}(t) - \mathbf{n}_\mathrm{c} \times \mathbf{r}(t)) - (\dot{\mathbf{r}}_\mathrm{e}(t) - \mathbf{n}_\mathrm{c} \times \mathbf{r}_\mathrm{e}(t)) \end{bmatrix}, \tag{19}$$

where

$$\mathbf{R}_I^H(t) = \mathbf{R}_z(-n_\mathrm{c}t)\mathbf{R}_x(-i_\mathrm{c})\mathbf{R}_z(-\dot{\Omega}t),$$

is the transformation from the ECI frame to the plane-rotating Hill's frame at the time t, and $\mathbf{R}_z \in \mathbf{SO}(\mathbf{3})$ and $\mathbf{R}_x \in \mathbf{SO}(\mathbf{3})$ are the rotations about z and x axis, respectively, where $\mathbf{SO}(\mathbf{3})$ is the special orthogonal group in dimension 3. Also, $\mathbf{n}_\mathrm{c} = [0 \;\; 0 \;\; n_\mathrm{c}]^\mathrm{T}$, and $\mathbf{r}_\mathrm{e}$ and $\dot{\mathbf{r}}_\mathrm{e}$ are the position vector in the ephemeris, respectively.

Summarizing, while the MPC prediction model is based on the Hill's equations under the approximations of a circular chief orbit which neglects non-keplerian perturbations, the initial condition is computed by the difference between the deputy orbit and the target orbit described by the ephemeris also accounting for the SSO orbital plane rotation. Note that although the ephemeris computation is in general very computationally demanding, since the ephemeris is the same over every repeat cycle for SSO, re-computation and re-uplink are not required. Also, the target orbit represented by the ephemeris, satisfies the conditions (13), (14) and (15).

B. Modifications to achieve also SSO Transferring

For transferring the SSO, a new ephemeris would normally need to be generated, but the re-propagation and re-uplink of it would require significant computational load and large data transfer volume. However, since the ephemeris is a time series dataset propagated under z-axially symmetrical gravity, time offsetting and rotation can be applied without the need of entire re-propagation, hence also avoiding re-uplink. The target angles $\Delta\phi$ and $\Delta\Omega$ are defined based on the ground trace, and the new ephemeris can generated by modifying (19) into

$$\mathbf{x}(\tau) = \begin{bmatrix} \mathbf{R}_I^H(t) & \mathbf{0} \\ \mathbf{0} & \dfrac{1}{n_\mathrm{c}}\mathbf{R}_I^H(t) \end{bmatrix} \begin{bmatrix} \mathbf{r}(t) - \mathbf{R}_z(\Delta\Omega)\mathbf{r}_\mathrm{e}(t-\Delta t_\phi) \\ (\dot{\mathbf{r}}(t) - \mathbf{n}_\mathrm{c}\times\mathbf{r}(t)) - \mathbf{R}_z(\Delta\Omega)(\dot{\mathbf{r}}_\mathrm{e}(t-\Delta t_\phi) - \mathbf{n}_\mathrm{c}\times\mathbf{r}_\mathrm{e}(t-\Delta t_\phi)) \end{bmatrix}, \tag{20}$$

where $\Delta t_\phi = \dfrac{\Delta\phi}{n_\mathrm{c}}$ represents the difference between the target LST and nominal LST. In this paper, we call the maneuver defined by $\Delta\phi$ as "in-trace maneuver" and $\Delta\Omega$ as "out-of-trace maneuver". An advantage of using (20) is that the computations are relatively simple, so that they can be operated on board the satellite.

C. Extensions for Handling Predictive Coasting and Underactuated Control

Usually, orbit control is disabled when the satellite instrumentation is operating, not to disturb the execution of the mission. However, external perturbations occur also during such time intervals, and may lead to the satellite being excessively far from its nominal orbit, preventing the mission success, given that the control is disabled. However, since the mission schedule is pre-determined, the MPC can exploit its prediction capabilities to minimize the impact of the perturbations before hand, by pre-compensating for the expected effect of the disturbances during the coasting phase. For allowing to represent also the coasting sections, the prediction model in the MPC (16) is modified again into

$$\bar{\mathbf{A}}_k = \begin{bmatrix} \mathbf{A}_\mathrm{D} & \mathbf{B}_\mathrm{D} & \mathbf{B}_\mathrm{D}\mathbf{S}(\tau_k) & \mathbf{0} \\ \mathbf{0} & \mathbf{I} & \mathbf{0} & \mathbf{0} \\ \mathbf{0} & \mathbf{0} & \mathbf{S}(\tau_k) & \mathbf{0} \\ \mathbf{E}(\tau_k) & \mathbf{0} & \mathbf{0} & \mathbf{I} \end{bmatrix}, \quad \bar{\mathbf{B}}_k = \begin{bmatrix} \mathbf{B}_\mathrm{D}\mathbf{S}(\tau_k) \\ \mathbf{0} \\ \mathbf{S}(\tau_k) \\ \mathbf{0} \end{bmatrix},$$

where $\mathbf{S} \in \mathbb{R}^{3\times3}$ is the matrix defined as

$$\mathbf{S}(\tau) = \begin{bmatrix} S_x(\tau) & 0 & 0 \\ 0 & S_y(\tau) & 0 \\ 0 & 0 & S_z(\tau) \end{bmatrix},$$

and S_x, S_y and S_z represent each component of the thrust $\mathbf{u}$ being active or not. For a coasting section scheduled from τ_s to τ_e, since all components of thrust are turned off, the elements of $\mathbf{S}$ are

$$S_x(\tau),\ S_y(\tau),\ S_z(\tau) = \begin{cases} 0 & (\tau_\mathrm{s} \le \tau \le \tau_\mathrm{e}) \\ 1 & (\tau \le \tau_\mathrm{s},\ \tau \ge \tau_\mathrm{e}). \end{cases} \tag{21}$$

Although this is not common in standard missions, equation (21) allows for selectively disabled. For instance, the orbit control can be conducted without x component of the thrust, in which case for de-activating u_x from τ_s to τ_e, the elements of $\mathbf{S}$ are

$$S_x(\tau) = \begin{cases} 0 & (\tau_\mathrm{s} \le \tau \le \tau_\mathrm{e}) \\ 1 & (\tau \le \tau_\mathrm{s},\ \tau \ge \tau_\mathrm{e}) \end{cases}, \quad S_y(\tau) = 1, \quad S_z(\tau) = 1.$$

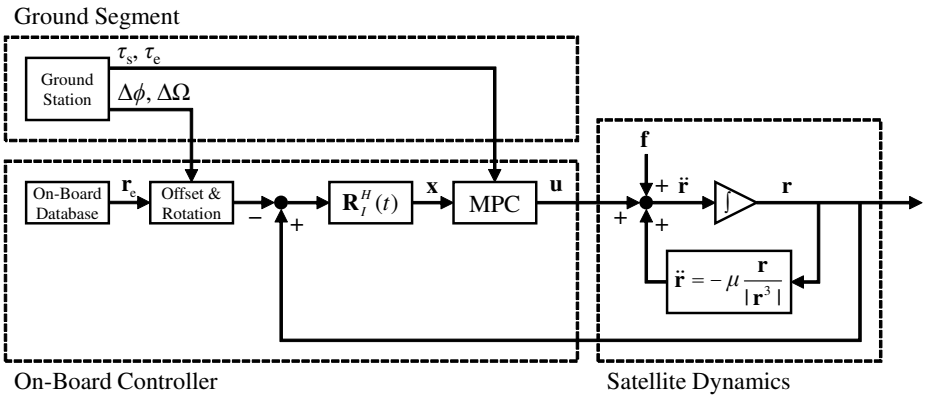

Fig. 4 System block diagram of LTV-MPC for SSO

D. LTV-MPC for SSO

At each sampling instant τ_k, MPC solves the finite horizon constrained optimal control problem

$$\min_{\Delta\mathbf{U}(\tau_k)} \quad \bar{\mathbf{x}}_{N|k}^{\mathrm{T}}\mathbf{P}\bar{\mathbf{x}}_{N|k} + \sum_{j=0}^{N-1} \bar{\mathbf{z}}_{j|k}^{\mathrm{T}}\mathbf{Q}\bar{\mathbf{z}}_{j|k} + \Delta\bar{\mathbf{u}}_{j|k}^{\mathrm{T}}\mathbf{R}\Delta\bar{\mathbf{u}}_{j|k} \tag{22a}$$

$$\text{s.t.} \quad \bar{\mathbf{x}}_{j+1|k} = \bar{\mathbf{A}}_{j|k}\bar{\mathbf{x}}_{j|k} + \bar{\mathbf{B}}_{j|k}\Delta\bar{\mathbf{u}}_{j|k} \tag{22b}$$

$$\bar{\mathbf{z}}_{j|k} = \bar{\mathbf{E}}_{j|k}\bar{\mathbf{x}}_{j|k} \tag{22c}$$

$$\bar{\mathbf{y}}_{j|k} = \bar{\mathbf{C}}_{j|k}\bar{\mathbf{x}}_{j|k} + \bar{\mathbf{D}}_{j|k}\Delta\bar{\mathbf{u}}_{j|k} \tag{22d}$$

$$\Delta\bar{\mathbf{u}}_{\min} \le \Delta\bar{\mathbf{u}}_{j|k} \le \Delta\bar{\mathbf{u}}_{\max} \tag{22e}$$

$$\bar{\mathbf{y}}_{\min} \le \bar{\mathbf{y}}_{j|k} \le \bar{\mathbf{y}}_{\max} \tag{22f}$$

$$\bar{\mathbf{x}}_{0|k} = [\mathbf{x}(\tau_k)^{\mathrm{T}} \ \mathbf{f}_{\mathrm{a}}^{\mathrm{T}} \ \mathbf{u}(\tau_{k-1})^{\mathrm{T}} \ \boldsymbol{\iota}(\tau_k)^{\mathrm{T}}]^{\mathrm{T}} \tag{22g}$$

where $N \in \mathbb{N}$ is the prediction horizon, $\Delta\mathbf{U}(\tau_k) = [\Delta\bar{\mathbf{u}}_{0|k} \ \cdots \ \Delta\bar{\mathbf{u}}_{N-1|k}]$, (22a) is the cost function, $\mathbf{Q} \in \mathbb{R}^{12\times12}$, $\mathbf{Q} \ge 0$, $\mathbf{R} \in \mathbb{R}^{3\times3}$, $\mathbf{R} > 0$ are positive (semi)definite weight matrices and $\mathbf{P} \ge 0$ is the positive semidefinite terminal cost matrix, which can be designed to achieve local stability [8], (22b), (22c) are the prediction model dynamics and performance outputs obtained as in Sections III.A, III.C, (22g) sets the state at the beginning of the prediction horizon where $x(\tau_k)$ obtained as in Sections III.A or III.B, and (22d), (22e), (22f) are the constrained output equation, and input and output constraints, respectively, to formulate constraints on thrust magnitude and rate, and possibly to define allowed ranges for the ROE. The notation $X_{j|k}$ denotes the prediction of X based on data at τ_k for j sampling periods ahead, i.e., X_{k+j}. Thus, the matrices and vectors of the prediction model implemented here are obtained based by predicting the orbital conditions based on the nominal orbit as

$$\bar{\mathbf{x}}_{j|k} = [\mathbf{x}(\tau_{k+j})^{\mathrm{T}} \ \mathbf{f}_{\mathrm{a}}^{\mathrm{T}} \ \mathbf{u}(\tau_{k+j-1})^{\mathrm{T}} \ \boldsymbol{\iota}(\tau_{k+j})^{\mathrm{T}}]^{\mathrm{T}}, \quad \bar{\mathbf{y}}_{j|k} = [\mathbf{z}(\tau_{k+j})^{\mathrm{T}} \ \mathbf{u}(\tau_{k+j})^{\mathrm{T}}]^{\mathrm{T}},$$

$$\bar{\mathbf{z}}_{j|k} = [\mathbf{z}_{\mathrm{g}}(\tau_{k+j})^{\mathrm{T}} \ \boldsymbol{\iota}(\tau_{k+j})^{\mathrm{T}}]^{\mathrm{T}}, \quad \Delta\bar{\mathbf{u}}_{j|k} = \mathbf{u}(\tau_{k+j}) - \mathbf{u}(\tau_{k+j-1}),$$

$$\bar{\mathbf{A}}_{j|k} = \begin{bmatrix} \mathbf{A}_{\mathrm{D}} & \mathbf{B}_{\mathrm{D}} & \mathbf{B}_{\mathrm{D}}\mathbf{S}(\tau_{k+j}) & \mathbf{0} \\ \mathbf{0} & \mathbf{I} & \mathbf{0} & \mathbf{0} \\ \mathbf{0} & \mathbf{0} & \mathbf{S}(\tau_{k+j}) & \mathbf{0} \\ \mathbf{E}_{\mathrm{g}}(\tau_{k+j}) & \mathbf{0} & \mathbf{0} & \mathbf{I} \end{bmatrix}, \quad \bar{\mathbf{B}}_{j|k} = \begin{bmatrix} \mathbf{B}_{\mathrm{D}}\mathbf{S}(\tau_{k+j}) \\ \mathbf{0} \\ \mathbf{S}(\tau_{k+j}) \\ \mathbf{0} \end{bmatrix},$$

$$\bar{\mathbf{C}}_{j|k} = \begin{bmatrix} \mathbf{E}_{\mathrm{g}}(\tau_{k+j}) & \mathbf{0} & \mathbf{0} & \mathbf{0} \\ \mathbf{0} & \mathbf{0} & \mathbf{I} & \mathbf{0} \end{bmatrix}, \quad \bar{\mathbf{D}}_{j|k} = \begin{bmatrix} \mathbf{0} \\ \mathbf{I} \end{bmatrix}, \quad \bar{\mathbf{E}}_{j|k} = \begin{bmatrix} \mathbf{E}_{\mathrm{g}}(\tau_{k+j}) & \mathbf{0} & \mathbf{0} & \mathbf{0} \\ \mathbf{0} & \mathbf{0} & \mathbf{0} & \mathbf{I} \end{bmatrix}.$$

For LTV-MPC the optimal control problem (22) can be formulated as a quadratic program, for which fast and memory efficient solvers exists [8]. Here we use the solver proposed in [24], which is very compact and still achieves the solution

in less than 0.05 seconds in our laptop, which is much smaller than the sampling period for the controller, hence indicating that the algorithm may take a small amount of the on-board computational capabilities.

Then, the MPC applies as control input to the satellite the command obtained from the first element of the optimal solution $\Delta\mathbf{U}^*(\tau_k)$ of (22),

$$\mathbf{u}(\tau_k) = \mathbf{u}(\tau_{k-1}) + \Delta\bar{\mathbf{u}}^*_{0|k}. \tag{23}$$

The resulting overall control architecture for the LTV-MPC for SSO is shown in Fig. 4.

IV. Satellite Simulations in Closed-loop with MPC for SSO Control

The behavior of the satellite controlled in closed-loop with LTV-MPC for SSO is verified by numerical simulations. The simulation conditions are shown in Table 1. The target orbit is a typical VLEO at an altitude of 274 km, for which the orbital period is 90 minutes, and the MPC prediction horizon is 108 minutes, slightly longer than one orbit, and the sampling period is 3 minutes, giving $N = 36$, which is in general appropriate [8].

Table 1 Simulation Conditions

Parameters	Values
Mean Altitude	274 km
Orbital Period	90 min
Repeat Cycle	1 day
Satellite Weight	500 kg
Cross-Sectional Area	15 m^2
Drag Coefficient	2.2
Maximum Thrust	0.1 N (Each Direction)
MPC Sampling Period	3 min
MPC Horizon	108 min ($N = 36$)

In Section IV.A, IV.C and IV.B, the simulation is based on the standard nonlinear models, in which it is assumed that the air density is constant and the gravitational perturbations are only J_2, J_3 and J_4. The ephemeris is calculated under J_2, J_3 and J_4 satisfying the SSO conditions (13) and (14) and the frozen condition (15). In Section IV.D, the orbit propagator, atmospheric model and geopotential model are provided by GMAT where we use the parameters shown in Table 2. The ephemeris is calculated under the geopotential model satisfying the conditions (13), (14), (15). In all cases, the initial state is set by $\mathbf{r}(0) = \mathbf{r}_e(0)$, $\dot{\mathbf{r}}(0) = \dot{\mathbf{r}}_e(0)$. In the following results, it should be noted that the ROE represents the difference between the deputy orbit and the target orbit.

Table 2 GMAT Settings

Parameters	Values
Propagator	PrinceDormand78
Atmospheric Model	MSISE90
Geopotential Model	EGM96
Other Bodies	Sun, Moon

A. Simulation of SSO Keeping

The comparison of time history of ROE, thrust and ground trace without control (free motion) and with control are shown in Fig. 5. Without control, the ROE were perturbed by the air drag. As a result, the relative semi-major axis Δa

decreases, and the satellite moves ahead due to the shorter period of the lower orbit. When the LTV-MPC is applied, after the initial transient where the predicted disturbance model and the integral action settle, the orbit is successfully kept within 1 meter. In the ground trace plots, the start position and end position are marked with circles. Without control, the satellite did not return to the start position due to the air drag perturbations, whereas the end position accurately matched the start position when MPC controls the satellite.

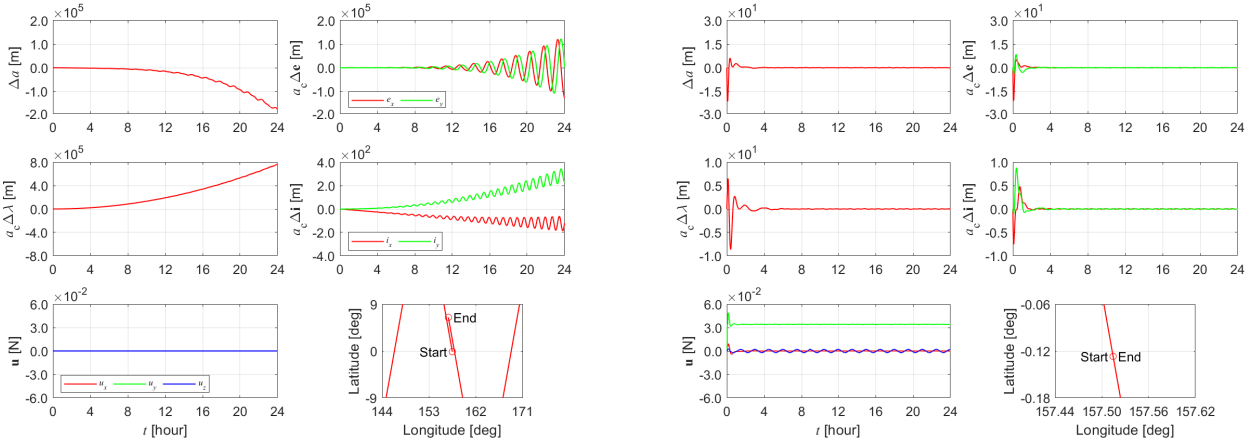

Fig. 5 Time history of ROE, thrust and ground trace. Left: without control (free motion). Right: with control.

The time history of ROE, thrust and ground trace for 3 days with control using a 1 day long ephemeris is shown in Fig. 6. Since the ephemeris is not dynamically continuous at the joint, the ROE show some deviations at the multiples of 24 hours. However, the MPC continued operating properly with the shifted ephemeris, which do not require re-computation and re-uplink.

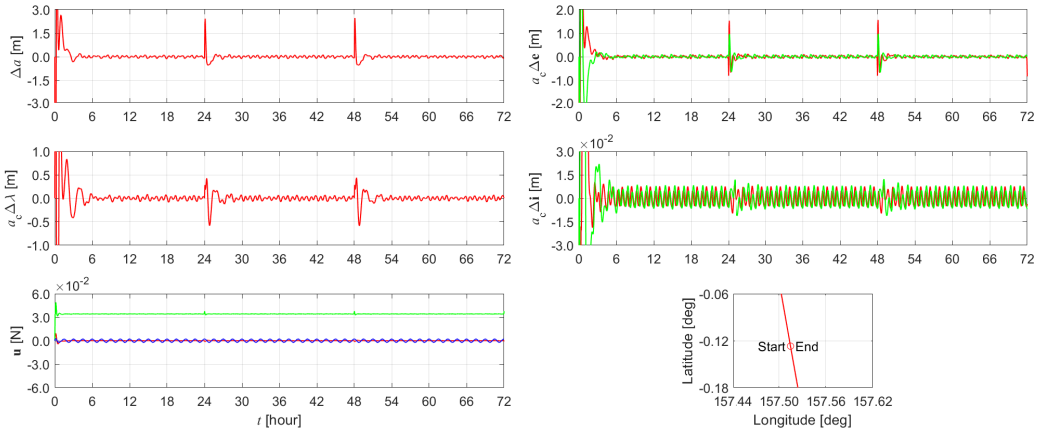

Fig. 6 Time history of ROE, thrust and ground trace for 3 days with control using 1 day long ephemeris.

B. Simulation of SSO Transferring

Next we simulated in-trace and out-of-trace SSO transfers. On an in-trace maneuver, the satellite should be shifted only in the along-trace direction, and the ground trace should be tracked due to the effect of (8). The comparison of time history and ground trace error for an in-trace maneuver when the ROE are considered as performance output, i.e., $\mathbf{E}$ as in (6), versus considering as performance output the ground trace tracking conditions (8), (9) formulated on ROE, i.e., $\mathbf{E}_g$ in (18) are shown in Fig. 7. Here, $\Delta\phi = 0.05$ deg was applied at $t = 4$ hours. Since the ROE represents the difference from the target orbit, the ROE jumped at $t = 4$ hours due to the change of target orbit. Although in both cases

the in-trace maneuver was completed successfully and the end point was shifted by 0.05 deg as requested, the impact on the the out-of-plane element $\Delta\mathbf{i}$ was different. Fig. 7 shows that the maximum ground trace error was reduced when $\mathbf{E}_g$ was used, compared to the when $\mathbf{E}$ was used.

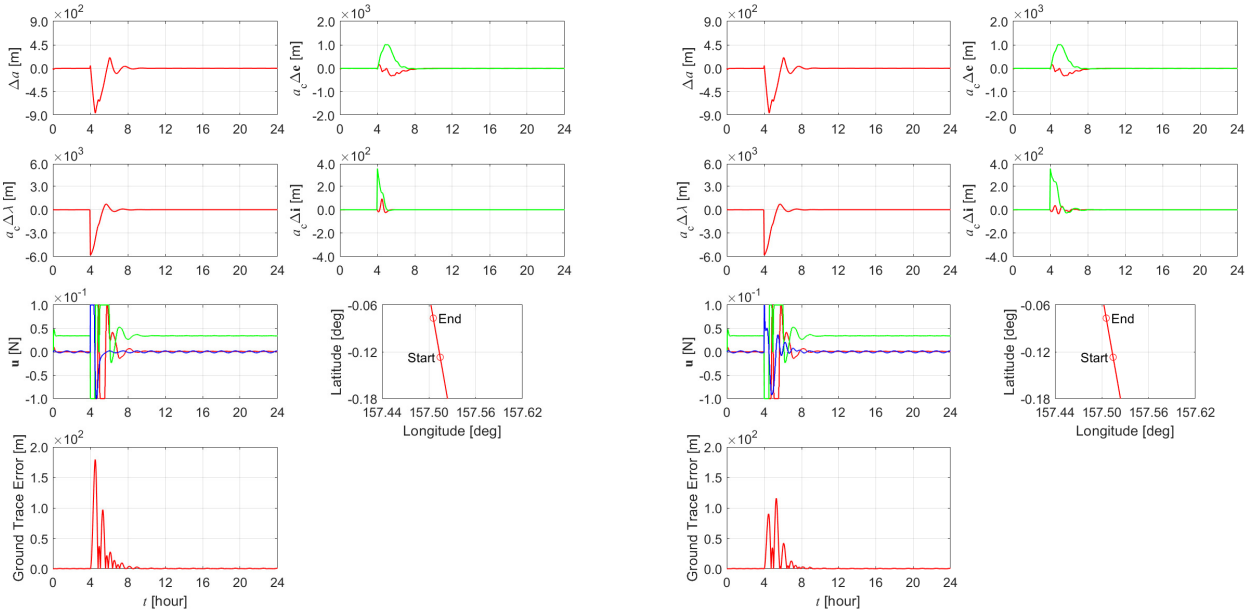

Fig. 7 Time history of ROE, thrust, ground trace and ground trace error. Left: in-trace maneuver with E. Right: in-trace maneuver with $\mathbf{E}_g$.

The time history of ROE, thrust and ground trace for an out-of-trace maneuver and for the combination of in-trace and out-of-trace maneuver are shown in Fig. 8, where $\Delta\Omega = 0.05$ deg and $\Delta\Omega$, $\Delta\phi = 0.05$ deg were applied at $t = 4$ hours, respectively. Both maneuvers were successfully completed, and the out-of-trace maneuver end point shifted by 0.05 deg in the longitude direction, while for the combined in-trace and out-of-trace maneuver the end point shifted by 0.05 deg in both the along-trace and longitude directions.

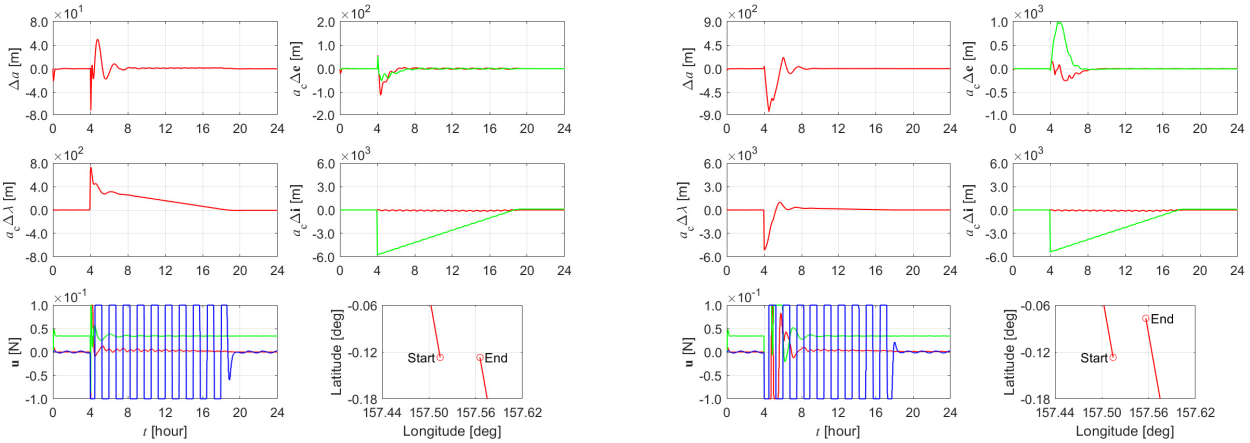

Fig. 8 Time history of ROE, thrust and ground trace. Left: out-of-trace maneuver. Right: combination of in-trace and out-of-trace maneuver.

C. Simulation of Predictive Coasting and Underactuated Control

The comparison of time history and ground trace of coasting without prediction and with prediction are shown in Fig. 9. Here, 30 minutes long coasting sections were applied at $t = 4.00,\ 5.25,\ 6.25,\ 7.00$ hours, as shown by the shaded sections in Fig. 9. Without prediction, the coasting section **S** were not defined in the prediction model yet the trust was cut off in the sections. As a result, the perturbations on the ROE would not be immediately compensated during these sections. On the other hand, when prediction information on the coasting sections is used, the MPC could reduce the maximum ROE error by maneuvering before the coasting sections. Also, the propellant consumption (amount of thrust) decreased due to the error reduction.

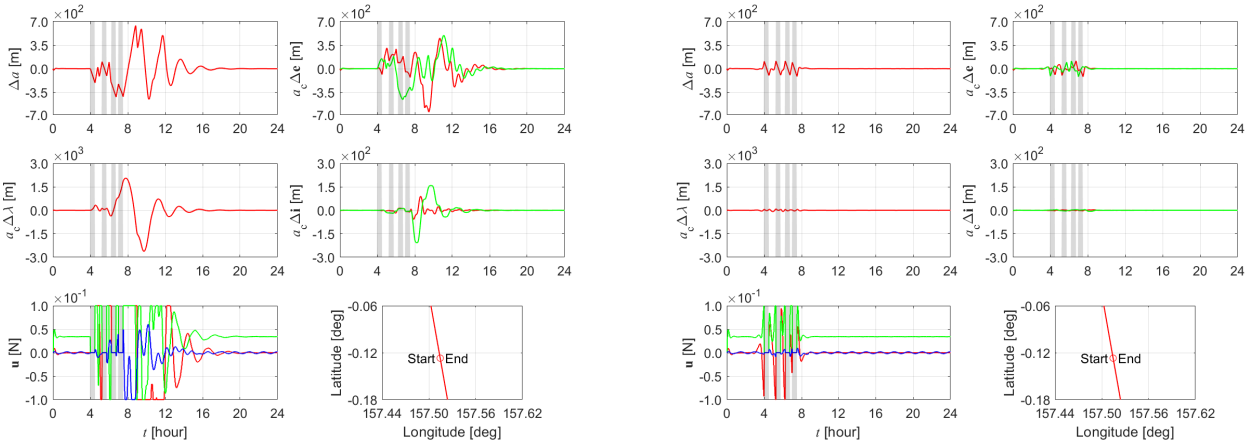

Fig. 9 Time history of ROE, thrust and ground trace. Left: coasting without prediction. Right: coasting with prediction.

We also evaluated the case where for a section starting at $t \geq 4.00$ hour, the x component of thrust was disabled yet the MPC can predict this. The result is shown in Fig. 10 where the section in which the x thrust is disabled is shown by the red shade. Due to the lack of u_x, the errors in ROE increased compared to Fig. 9. However, the MPC could still control the satelllite despite it being underactuated.

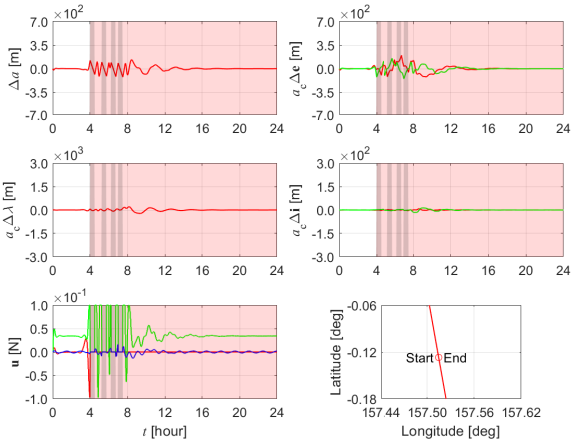

Fig. 10 Time history of ROE, thrust and ground trace of coasting with underactuated control, both predicted.

D. Simulations in closed-loop with GMAT Model

Next, we show the results of validating some of the maneuvers previously simulated with the nonlinear model (1) by using MPC in closed-loop with the simulation model in GMAT obtained according to the parameters in Table 2. The

time history of ROE, thrust and ground trace for 3 days using a 1 day long ephemeris simulated is shown in Fig. 11. Also, the results of the combination of in and out-of-trace maneuver and coasting with prediction are shown in Fig. 12. Due to the detailed atmospheric model (MSISE90), geopotential model (EGM96) and other bodies' gravity, the orbit was periodically disturbed, and the thrust oscillated. However, the orbit was successfully kept within 15 meters. Also, although the transient was slightly longer than the result based on the simple nonlinear model (1), SSO transferring and predictive coasting were properly conducted. These results, based on a more detailed and validated model, provide additional indications of the effectiveness of the LTV-MPC approach for SSO.

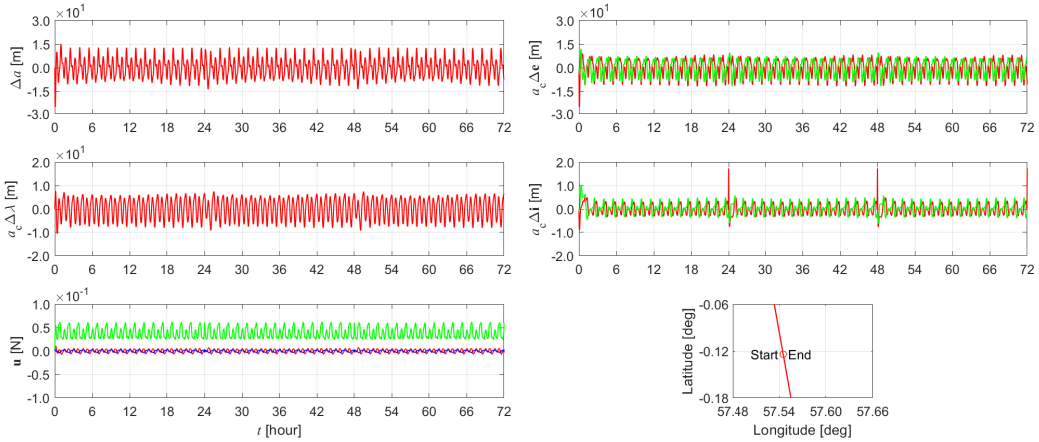

Fig. 11 Time history of ROE, thrust and ground trace for 3 days with control using 1 day long ephemeris for MPC simulated in closed-loop with GMAT.

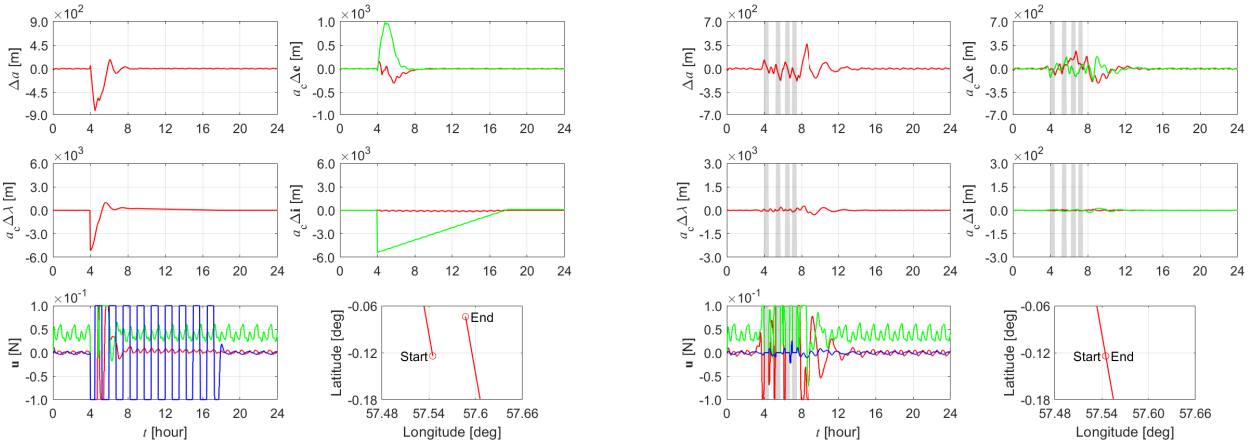

Fig. 12 Time history of ROE, thrust and ground trace for MPC simulated in closed-loop with GMAT. Left: combination of in-trace and out-of-trace maneuver. Right: coasting with prediction.

V. Conclusions

In this paper, we have proposed a design for satellite control on SSO by the LTV-MPC using ROE. In order for the controller to reject the air drag perturbation while still exploiting the J_2 term of the Earth gravitational perturbation to achieve SSO, we have introduced ephemeris, and the plane-rotating Hill's frame transformation for computing the initial condition for the MPC prediction at each sampling instant.

The MPC enables orbit keeping and transferring, and the predictive features of MPC allow for minimizing the impact of the perturbations during the coasting sections where the mission is usually carried out. By properly

formulating the performance output with respect to the ROE, the ground trace error can be reduced and the LST can be precisely controlled. Since the MPC only requires solving convex quadratic program, it appears suitable for on-board implementation and hence it appears appealing for autonomous satellite control, especially in VLEO, without needing to resort to the ground stations.

References

[1] De Lisle, D., Iris, S., Arsenault, E., Smyth, J., and Kroupnik, G., "RADARSAT Constellation Mission Status Update," *12th European Conference on Synthetic Aperture Radar*, 2018.

[2] Thompson, A. A., "Overview of the RADARSAT Constellation Mission," *Canadian Journal of Remote Sensing*, 2015.

[3] Imamura, S., Utashima, M., Ozawa, T., Akiyama, K., and Sasaki, M., "Current status of the on-going orbit transfer of Super Low Altitude Test Satellite (SLATS)," *69th International Astronautical Congress*, 2018.

[4] Kawasaki, H., Konoue, K., Hoshino, H., Kaneko, Y., and Sasaki, M., "Interim Report of Super Low Altitude Satellite Operation," *2018 IEEE International Geoscience and Remote Sensing Symposium*, 2018.

[5] Noda, A., Homma, M., and Utashima, M., "The Study of a Super Low Altitude Satellite," *26th International Symposium on Space Technology and Science*, 2008.

[6] NOAA, NASA, and USAF, *U.S. Standard Atmosphere, 1976*, United States, 1976.

[7] D'Amico, S., *Relative Orbital Elements as Integration Constants of the Hill's Equations*, Deutsches Zentrum für Luft- und Raumfahrt, 2005.

[8] Di Cairano, S., and Kolmanovsky, I. V., "Real-time optimization and model predictive control for aerospace and automotive applications," *American Control Conference*, 2018, pp. 2392–2409.

[9] Eren, U., Prach, A., Koçer, B. B., Raković, S. V., Kayacan, E., and Açıkmeşe, B., "Model Predictive Control in Aerospace Systems: Current Stateand Opportunities," *Journal of Guidance, Control, and Dynamics*, 2017.

[10] Di Cairano, S., Park, H., and Kolmanovsky, I., "Model Predictive Control Approach for Guidance of Spacecraft Rendezvous andProximity Maneuvering," *International Journal of Robust and Nonlinear Control*, 2012.

[11] Weiss, A., Baldwin, M., Erwin, R. S., and Kolmanovsky, I., "Model Predictive Control for Spacecraft Rendezvous and Docking: Strategies for Handling Constraints and Case Studies," *IEEE Transactions on Control Systems Technology*, 2015.

[12] Caverly, R. J., Di Cairano, S., and Weiss, A., "Control Allocation and Quantization of a GEO Satellite with 4DOF Gimbaled Thruster Booms," *AIAA Scitech Forum*, 2020.

[13] Caverly, R. J., Di Cairano, S., and Weiss, A., "Split-Horizon MPC for Coupled Station Keeping, Attitude Control, and Momentum Management of GEO Satellitesusing Electric Propulsion," *American Control Conference*, 2018.

[14] Kalabić, U., Weiss, A., Kolmanovsky, I. V., and Di Cairano, S., "Station-keeping and momentum-management on halo orbitsaround L2: Linear-quadratic feedback andmodel predictive control approaches," *Advances in Astronautics Science and Technology*, 2015.

[15] Hughes, S. P., *General Mission Analysis Tool (GMAT)*, Goddard Space Flight Center, 2016.

[16] Hughes, S. P., Qureshi, R. H., Cooley, D. S., Parker, J. J. K., and Grubb, T. G., "Verification and validation of the general mission analysis tool (GMAT)," *AIAA/AAS Astrodynamics Specialist Conference*, 2014.

[17] Curtis, H. D., *Orbital Mechanics for Engineering Students*, Butterworth-Heinemann, 2014.

[18] Schaub, H., and Junkins, J. L., *Analytical Mechanics of Space Systems, Fourth Edition*, American Institute of Aeronautics and Astronautics, 2018.

[19] Clohessy, W., and Wiltshire, R., "Terminal Guidance System for Satellite Rendezvous," *Journal of the Aerospace Sciences*, 1960.

[20] Sullivan, J., Grimberg, S., and D'Amico, S., "Comprehensive Survey and Assessment of Spacecraft Relative Motion Dynamics Models," *Journal of Guidance, Control, and Dynamics*, 2017.

[21] Dang, Z., and Zhang, H., "Linearized relative motion equations through orbital element differences for general Keplerian orbits," *Astrodynamics*, 2018.

[22] D'Amico, S., and Montenbruck, O., "Proximity Operations of Formation-Flying Spacecraft Using an Eccentricity/Inclination Vector Separation," *Journal of Guidance, Control, and Dynamics*, 2006.

[23] Gaias, G., and D'Amico, S., "Impulsive Maneuvers for Formation Reconfiguration Using Relative Orbital Elements," *Journal of Guidance, Control, and Dynamics*, 2015.

[24] Raghunathan, A. U., and Di Cairano, S., "Optimal step-size selection in alternating direction method of multipliers for convex quadratic programs and model predictive control," *Proc. Symp. mathematical theory of networks and systems*, 2014, pp. 807–814.